THE JOURNAL OF BIOLOGICAL CHEMISTRY

Vol. 260, No. 21, Issue of September 25, pp. 11730-11743, 1985
Printed in U.S.A.

# Crystallization of the $Ca^{2+}$-ATPase of Sarcoplasmic Reticulum by Calcium and Lanthanide Ions*

(Received for publication, February 25, 1985)

**Laszlo Dux‡§, Kenneth A. Taylor¶, H. Ping Ting-Beall¶, and Anthony Martonosi‖****

*From the ‡‖Department of Biochemistry, State University of New York, Upstate Medical Center, Syracuse, New York 13210 and the ¶Department of Anatomy, Duke University Medical Center, Durham, North Carolina 27710*

**Two-dimensional crystalline arrays of $Ca^{2+}$-ATPase molecules develop in sarcoplasmic reticulum vesicles exposed to $Ca^{2+}$ or lanthanide ions. The $Ca^{2+}$- or lanthanide-induced crystals are presumed to represent the $E_1$ conformation of the $Ca^{2+}$-ATPase, and their crystal form is clearly different from the earlier described $E_2$ crystals induced by $Na_3VO_4$ in the presence of ethylene glycol bis(β-aminoethyl ether)-*N,N,N',N'*-tetraacetic acid (Taylor, K. A., Dux, L., and Martonosi, A. (1984) *J. Mol. Biol.* 174, 193–204). Analysis of the crystalline arrays by negative staining or freeze-fracture electron microscopy reveals obliquely oriented rows of particles corresponding to individual $Ca^{2+}$-ATPase molecules. Computer analysis of the negatively stained lanthanide-induced crystalline $Ca^{2+}$-ATPase arrays shows that the molecules are arranged in a P1 lattice. The pear-shaped profiles of $Ca^{2+}$-ATPase molecules seen in projection in the density maps are similar to those seen in vanadate-induced crystals. The space group and unit cell dimensions of the $E_1$ crystals are consistent with $Ca^{2+}$-ATPase monomers as structural units, while the vanadate-induced $E_2$ crystals form by lateral aggregation of chains of $Ca^{2+}$-ATPase dimers. The transition between the $E_1$ and $E_2$ conformations may involve a shift in the monomer-oligomer equilibrium of the $Ca^{2+}$-ATPase. The formation of $E_1$ crystals by $PrCl_3$ is promoted by inside negative membrane potential, presumably through stabilization of the $E_1$ conformation of the enzyme. Cleavage of the $Ca^{2+}$-ATPase by trypsin into two major fragments (A and B) did not interfere with the $Ca^{2+}$- or the $Pr^{3+}$-induced crystallization.**

The ATP-dependent transport of calcium by the sarcoplasmic reticulum is initiated by the binding of $Ca^{2+}$ and ATP to the $Ca^{2+}$ transport ATPase in the $E_1$ conformation (Martonosi and Beeler, 1983). This is followed by the phosphorylation of an aspartyl group in the active site and the conversion of the enzyme from the $E_1$ into the $E_2$ form, accompanied by the transfer of $Ca^{2+}$ across the membrane. The cycle is completed by the release of $Ca^{2+}$ on the luminal side and the hydrolysis of the phosphoenzyme intermediate, yielding inorganic phosphate.

The alternation between the two distinct conformations of $Ca^{2+}$-ATPase during the transport cycle is supported by changes in the affinity of the enzyme for $Ca^{2+}$, $Mg^{2+}$, ATP, and ADP (Martonosi, 1982), the differences in the reactivity of protein functional groups (Ikemoto, 1982), and the responses of fluorescence (Dupont *et al.*, 1982) and electron spin resonance probes (Inesi *et al.*, 1982) at predicted stages in the $Ca^{2+}$ transport process.

Vanadate (V) ions stabilize the $Ca^{2+}$-ATPase in the $E_2$ conformation (Pick, 1982; Pick and Karlish, 1982). Therefore the $Ca^{2+}$-ATPase crystals induced by $Na_3VO_4$ in sarcoplasmic reticulum (Dux and Martonosi, 1983a, 1983b, 1983c, 1983d) are expected to reflect the geometry of ATPase-ATPase interactions characteristic of the $E_2$ conformation.

Here we report the formation of a new crystal form of the $Ca^{2+}$-ATPase that is observed in sarcoplasmic reticulum vesicles exposed to $10^{-5}$–$10^{-4}$ M $Ca^{2+}$, or $10^{-6}$–$10^{-5}$ M lanthanides, at a slightly alkaline pH. $Ca^{2+}$ and lanthanides are presumed to bind to the $Ca^{2+}$-ATPase in the $E_1$ conformation (Grisham, 1982). Therefore the crystals formed under these conditions probably arise from interaction between $Ca^{2+}$-ATPase molecules in the $E_1$ form.

Preliminary reports of this work appeared (Dux *et al.*, 1984; Martonosi *et al.*, 1985).

## EXPERIMENTAL PROCEDURES

Sarcoplasmic reticulum vesicles were prepared from predominantly white skeletal muscles of rabbit (Nakamura *et al.*, 1976). The vesicles were suspended in 0.25 M sucrose, 10 mM Tris maleate, pH 7.4, solution at a concentration of 25 mg of protein/ml and stored at −70 °C for several weeks until use. The protein composition of the vesicles was analyzed by sodium dodecyl sulfate-polyacrylamide gel electrophoresis on 6–18% gradient gels, as described earlier (Dux and Martonosi, 1983b). Protein was determined according to Lowry *et al.* (1951).

For the formation of $Ca^{2+}$-ATPase crystals the vesicle suspensions were diluted to a final concentration of 1 mg of protein/ml in a medium of 0.1 M KCl, 10 mM imidazole, pH 8.0, and 5 mM $MgCl_2$ at 2 °C. Crystallization was induced by the addition of $Ca^{2+}$ or lanthanides to the above crystallizing medium. Incubation at 2 °C ranged from a few hours to several days.

### *Electron Microscopy*

*Negative Stain*—Specimens for electron microscopy were prepared in one of two ways. For routine observations vesicle suspensions were deposited on carbon coated parlodion films, negatively stained with 1% uranyl acetate and viewed on a Siemens-Elmiskop 102 electron microscope operated at 60 kV. The praseodymium-induced crystals used in the image analysis were deposited on carbon films prepared from a freshly cleaved mica surface and stained with 2% uranyl acetate. The latter were examined on a Philips EM420 electron microscope operated at 100 kV accelerating voltage. Due to the relatively low number of well ordered crystalline tubules in the preparations, low dose microscopy was not attempted in the collection

* This work was supported by grants from the National Institutes of Health (AM 26545, GM 30598, GM 27804, and 1-S10-RR002283), the National Science Foundation (PCM84-03679 and PCM84-00167), the Muscular Dystrophy Association, the R. J. Reynolds Tobacco Co., and by an established investigatorship (to K. A. T.) from the American Heart Association. The costs of publication of this article were defrayed in part by the payment of page charges. This article must therefore be hereby marked "*advertisement*" in accordance with 18 U.S.C. Section 1734 solely to indicate this fact.

§ On leave from the Institute of Biochemistry, University Medical School, Szeged, Hungary.

** To whom all correspondence should be addressed.

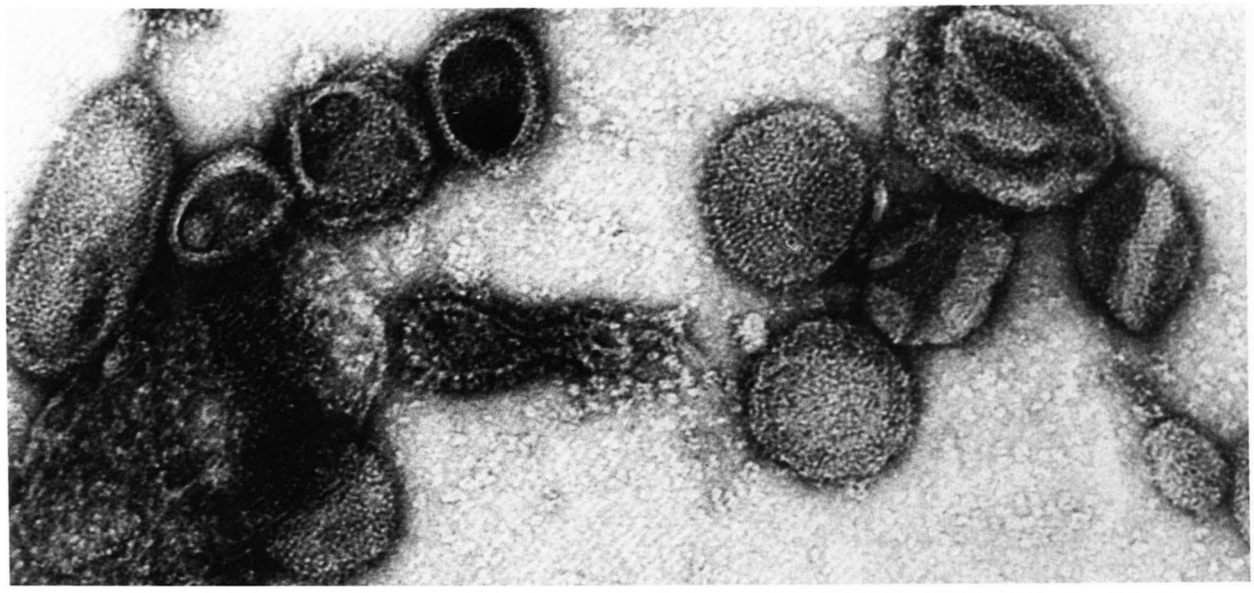

FIG. 1. **Crystalline arrays of $Ca^{2+}$-ATPase molecules induced by $Ca^{2+}$.** Sarcoplasmic reticulum vesicles were incubated with Chelex chelating resin (100 mg of wet resin/mg of protein) at 2 °C overnight with gentle stirring to chelate some of the endogenous calcium. After brief centrifugation in a clinical centrifuge the microsomes were diluted into a Chelex-treated medium of 0.1 M KCl, 10 mM imidazole, pH 8.0, to a final protein concentration of 1 mg/ml. $MgCl_2$ (5 mM) and $CaCl_2$ (100 $\mu$M) were added and the incubation continued for 16 h at 2 °C, followed by negative staining with 1% uranyl acetate. Note the evenly spaced single strands of $Ca^{2+}$-ATPase molecules that form a helical array around the more elongated tubules. In end-on view of the stain-filled vesicles, the bilayer contours are clearly outlined, with the 40-Å diameter ATPase particles projecting 50–60 Å into the cytoplasmic space. In favorable regions, the ATPase particles appear to be connected by stain-excluding structures that are located above the surface of the bilayer. Although crystalline arrays are seen on the surface of only about 10–15% of the vesicles, the crystalline vesicles are usually clustered in distinct regions of the grids. This suggests that the preservation of the crystals by the negative stain varies, and under optimal conditions for staining the fraction of the vesicles bearing crystals may be greater than 15%. In the middle of the picture, for comparison, a submitochondrial fragment is included with the 120-Å diameter $F_1$ particles projecting outward. Magnification: times 200,000.

of data for the praseodymium crystals. However, every attempt was made to photograph crystals quickly to minimize the effects of radiation damage.

*Freeze-Fracture*—Sarcoplasmic reticulum membranes, after exposure to $10^{-5}$ M $PrCl_3$ or 0.5 mM $CaCl_2$, were either fixed in 2% glutaraldehyde overnight or unfixed and rapidly frozen without cryoprotectant in liquid propane (Costello and Corless, 1978). Frozen samples were fractured in a Cryofract FFE device, model 190 (Reichert-Jung, Paris, France) at −170 °C and $2.5 \times 10^{-9}$ Torr, and replicated immediately with Pt/C at a 20 ° angle, followed by C at a 90 ° angle. The thickness of Pt and C was measured to be 9–11 Å and 110–120 Å, respectively, by a Maxtek thickness monitor model TM-100 (Maxtek Inc., Torrance, CA). The replicas were examined in a Philips 301 electron microscope at 80 kV using a 30-$\mu$m objective aperture.

### *Image Analysis*

Micrographs were screened by optical diffraction and a subset of images showing sharp diffraction spots was selected for computer processing. These were digitized on a Perkin-Elmer PDS 1010M microdensitometer at step sizes of 5.1–7.5 Å depending upon plate magnification. Digitized micrographs were processed as previously described (Taylor *et al.*, 1984).

### *Materials*

$NdCl_3$, $HoCl_3$, $PrCl_3$, $TbCl_3$, and $YbCl_3$ were obtained from Alfa Products, Danvers, MA. $LaCl_3$ and choline chloride were supplied by Fisher, $GdCl_3$ by Aldrich, and L-glutamic acid, trypsin (bovine pancreas), trypsin inhibitor (soybean), ATP, AMP-PNP,[1] and AMP-PCP, by Sigma. Acrylamide, *N,N′*-methylenebisacrylamide, sodium dodecyl sulfate, TEMED, and ammonium persulfate were obtained from Bio-Rad.

[1] The abbreviations used are: AMP-PNP, adenyl-5′-yl imidodiphosphate; TEMED, *N,N,N′,N′*-tetramethylethylenediamine; EGTA, ethylene glycol bis(β-aminoethylether)-*N,N,N′,N′*-tetraacetic acid; AMP-PCP, adenosine 5′-(β,γ-methylene)triphosphate.

## RESULTS

### *Membrane Crystals of $Ca^{2+}$-ATPase Induced by $Ca^{2+}$*

Ordered arrays of $Ca^{2+}$-ATPase molecules develop in sarcoplasmic reticulum vesicles suspended in 0.1 M KCl, 10 mM imidazole, pH 8.0, 5 mM $MgCl_2$, and $10^{-4}$ M $CaCl_2$ at 2 °C for 12–18 h (Fig. 1). The optimal free $Ca^{2+}$ concentration for "crystallization" is broad, ranging between $10^{-5}$ and $10^{-4}$ M, based on experiments with $Ca^{2+}$-EGTA buffer systems. Extended arrays develop on the surface of about 10–15% of the vesicle population. Addition of 5 mM ATP causes the disappearance of the $Ca^{2+}$-induced crystals, presumably because the rapid cyclic changes in enzyme conformation connected with $Ca^{2+}$ transport do not permit the development of stable interactions between ATPase molecules.

### *Crystallization of $Ca^{2+}$-ATPase by Lanthanides*

Binding of lanthanides to the $Ca^{2+}$ transport ATPase of sarcoplasmic reticulum competitively inhibits the $Ca^{2+}$ binding (Chevallier and Butow, 1971; Highsmith and Head, 1983; Itoh and Kawakita, 1984), and reduces the rate of ATP hydrolysis (Yamada and Tonomura, 1972; Krasnow, 1972, 1977; dos Remedios, 1977; Chiesi and Inesi, 1979; Stephens and Grisham, 1979, 1980; Grisham, 1982), with inhibition of the rate of formation and decomposition of the phosphoprotein intermediate (E ~ P) (Chiesi and Inesi, 1979; Stephens and Grisham, 1979; Itoh and Kawakita, 1984). These observations are consistent with the proposition that lanthanides, like $Ca^{2+}$, stabilize the $Ca^{2+}$-ATPase in the $E_1$ conformation.

Indeed $Gd^{3+}$ (Fig. 2), $La^{3+}$ (Fig. 3), $Pr^{3+}$, $Nd^{3+}$, $Tb^{3+}$, $Yb^{3+}$,

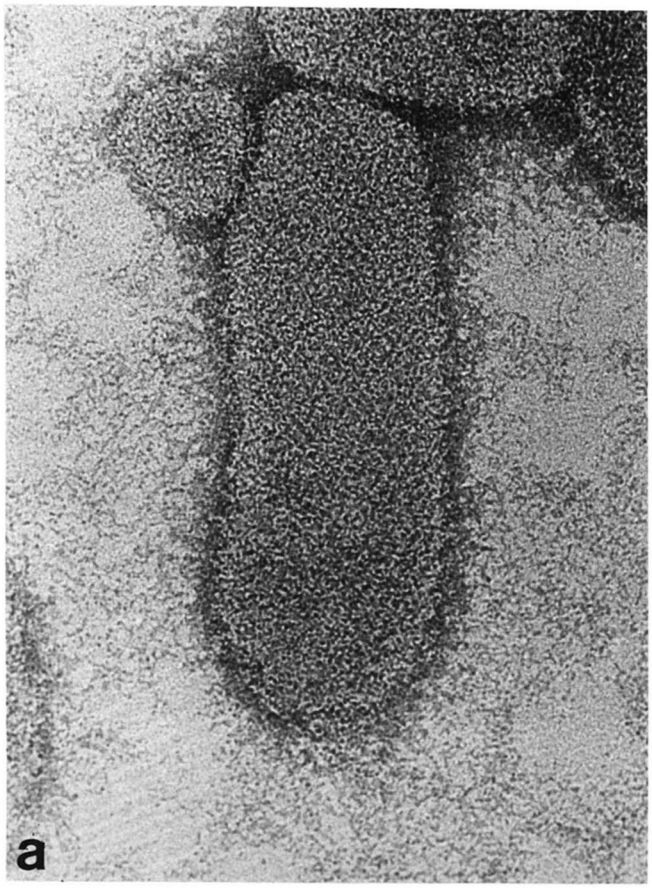


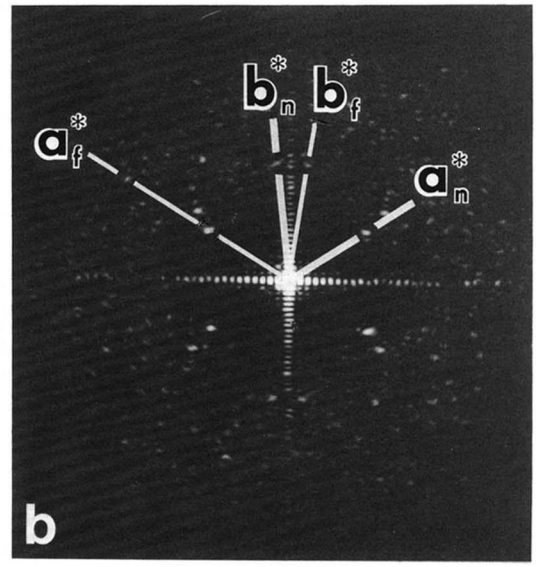


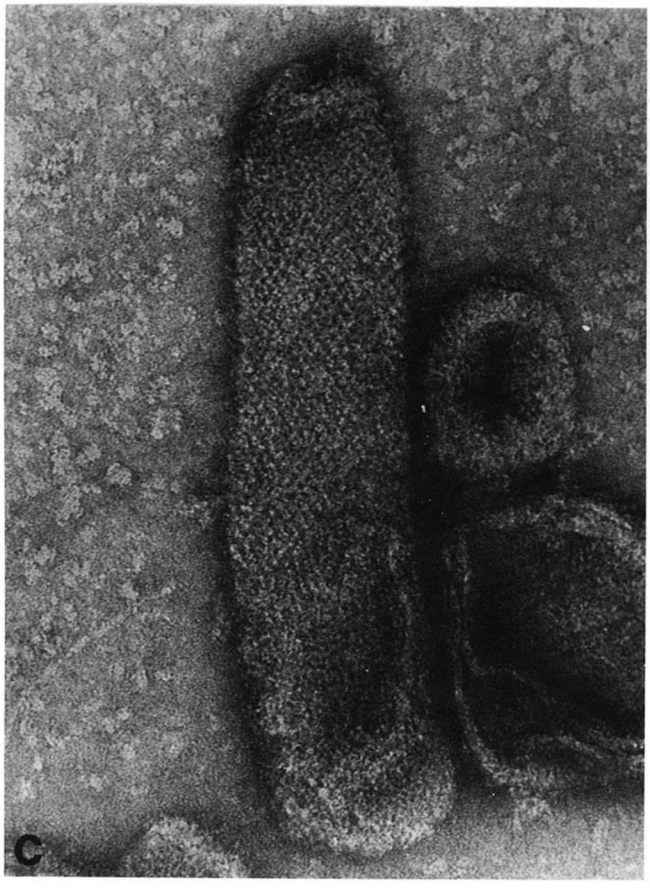


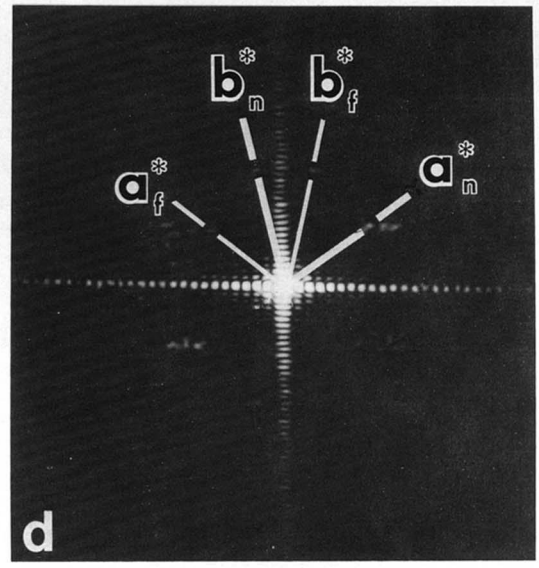


FIG. 2.

FIG. 3. **$Ca^{2+}$-ATPase crystals induced by $LaCl_3$.** $Ca^{2+}$-ATPase crystals were induced in sarcoplasmic reticulum vesicles suspended in 0.1 M KCl, 10 mM imidazole, pH 8.0, and 5 mM $MgCl_2$, by $LaCl_3$ (1 $\mu$M) at 2 °C. Individual ATPase molecules are well resolved in lateral projection around the periphery of stain-filled vesicles. Magnification: times 200,000.

and $Ho^{3+}$ (Figs. 2 and 4) effectively promote the crystallization of the $Ca^{2+}$-ATPase in sarcoplasmic reticulum vesicles at 2 °C. With $Pr^{3+}$, $Gd^{3+}$, and $La^{3+}$ the optimal concentration for crystallization was 6–8 $\mu$M, corresponding to about 1 mol of lanthanide/mol of $Ca^{2+}$ transport ATPase.

The crystal forms obtained with lanthanides and with $Ca^{2+}$ are similar and presumably reflect the $E_1$ conformation of the $Ca^{2+}$-ATPase. Therefore in subsequent discussion the lanthanide and $Ca^{2+}$-induced $Ca^{2+}$-ATPase crystals will be designated simply as $E_1$ crystals, to distinguish them from the earlier described $E_2$ crystals produced by vanadate in a $Ca^{2+}$-free medium (Dux and Martonosi, 1983a, 1983b, 1983c, 1983d; Taylor *et al.*, 1984).

Local disruptions of the membrane surfaces and sharp angles in the membrane profiles without the unwinding of the ATPase chains suggests that the crystalline vesicles obtained with $Gd^{3+}$, $La^{3+}$, or $Pr^{3+}$ are fragile and break under the shear stress of negative staining. Such disruptions have been observed only rarely in native vesicles or in vanadate-induced ($E_2$) ATPase crystals. Instead, the $E_2$ crystals had a tendency to unwind into isolated chains of dimers under conditions that promoted osmotic lysis of the vesicles (Dux and Martonosi, 1983c).

$E_1$-type crystals are observed in about 20–30% of the vesicles in the presence of 5 $\mu$M $Pr^{3+}$. This estimate is less accurate than the corresponding figures for the vanadate-induced $E_2$ crystals (Dux and Martonosi, 1983c) because of the apparent tendency of the $Pr^{3+}$ crystals to undergo fragmentation. Based on the fact that $E_2$-type crystals appear in 70–80% of the vesicles, we concluded earlier (Dux and Martonosi, 1984) that about 20–30% of the vesicle population in conventional sarcoplasmic reticulum preparations isolated from fast-twitch muscle may represent contaminating membrane elements derived from the surface membranes, T-tubules and to a lesser extent from mitochondria. These observations lead to the conclusion that $E_1$-type crystals are not seen in a significant portion of the vesicle population that can develop $E_2$ crystals and therefore originates from the sarcoplasmic reticulum. The unusual sensitivity of the $E_1$ crystals to the conditions of negative staining is supported by the observation that the largest and best organized crystalline arrays occur close to the grid bars, where the drying of the negative stain occurs at a slower rate. In these areas the fraction of vesicles covered with $E_1$-type crystals accounts for 60–70% of the vesicle population, *i.e.* nearly all vesicles derived from the sarcoplasmic reticulum crystallize.

### *Freeze-Fracture Electron Microscopy of the $E_1$ Crystals of $Ca^{2+}$-ATPase*

Crystalline arrays of intramembranous particles can be demonstrated in sarcoplasmic reticulum preparations exposed to $Ca^{2+}$ and lanthanides (Fig. 5) under similar conditions to those used for the demonstration of surface arrays by negative staining. The intramembranous particles are more numerous on the concave P (protoplasmic) faces than on the convex tubular faces of the membrane, in agreement with earlier observations (for review, see Martonosi and Beeler, 1983), suggesting that much of the mass of the $Ca^{2+}$ transport ATPase is associated with the cytoplasmic leaflet of the bilayer.

The $E_1$ crystals shown by freeze-fracture electron microscopy (Fig. 5) display rows of individual particles of ≃60-Å diameter on the P face, oriented obliquely. The size of the

FIG. 2. **Micrographs and optical diffraction patterns of lanthanide-induced $Ca^{2+}$-ATPase crystals.** *a* and *b*, praseodymium-induced crystalline array and its optical diffraction. Despite less detail in the image itself, these lower dose images constantly gave better diffraction patterns (*b*) than the higher dose images of the gadolinium crystals shown below. *c* and *d*, gadolinium-induced crystalline array and its optical diffraction pattern. The image is a complex superposition of the lattices from the top and bottom of the flattened crystalline tubule. Likewise the diffraction pattern (*d*) shows two lattices, one from the top, the other from the bottom side. Micrographs, 276,000 × magnification.

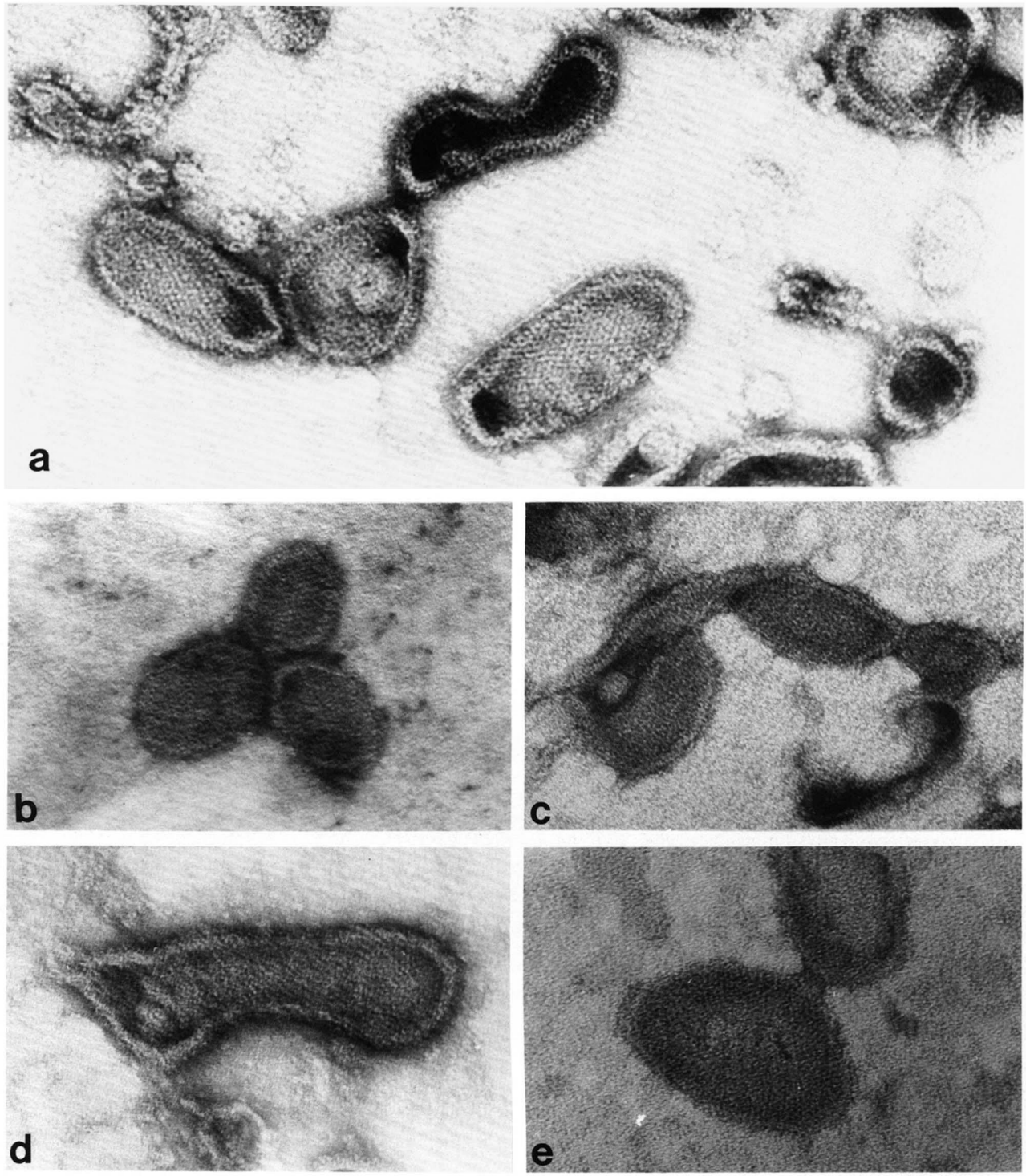


FIG. 4. **Ordered arrays of $Ca^{2+}$-ATPase particles induced by various lanthanide ions.** Sarcoplasmic reticulum vesicles were incubated in 0.1 M KCl, 10 mM imidazole, pH 8.0, 5 mM $MgCl_2$, and $10^{-6}$ M $PrCl_3$ (*a*), $NdCl_3$ (*b*), $TbCl_3$ (*c*), $YbCl_3$ (*d*), and $HoCl_3$ (*e*) at 2 °C for 16 h. Negative staining with 1% uranyl acetate. The main features of the lattice are similar with all lanthanides, but the order of crystalline arrays and the frequency of their occurrence appears slightly less with $Nd^{3+}$, $Tb^{3+}$, $Yb^{3+}$, and $Ho^{3+}$, than with $Pr^{3+}$, $Gd^{3+}$, or $La^{3+}$. Magnification: times 200,000.

particles on the concave P face appears generally smaller than the 75–85 Å normally reported (Martonosi and Beeler, 1983). This difference can be explained by the amount of metal used in replication. In the Cryofract replicas shown here, only 9–11 Å of Pt was used, compared to 25–40 Å in more conventional procedures. The ridges of particles seen on the P face of the $E_2$ crystals (Peracchia *et al.*, 1984) are not evident in the $E_1$ crystals. In some areas, particles are missing from the regular lattices and the spacings appear larger (≃120 Å, Fig. 5, *b* and *d*). Complementary oblique furrows on the convex E face, a characteristic feature of $E_2$ crystals (Peracchia *et al.*, 1984), are never observed in $E_1$ crystals. However, rows of pits oriented obliquely are visible (as indicated by *arrows* in Fig. 5, *a* and *e*).

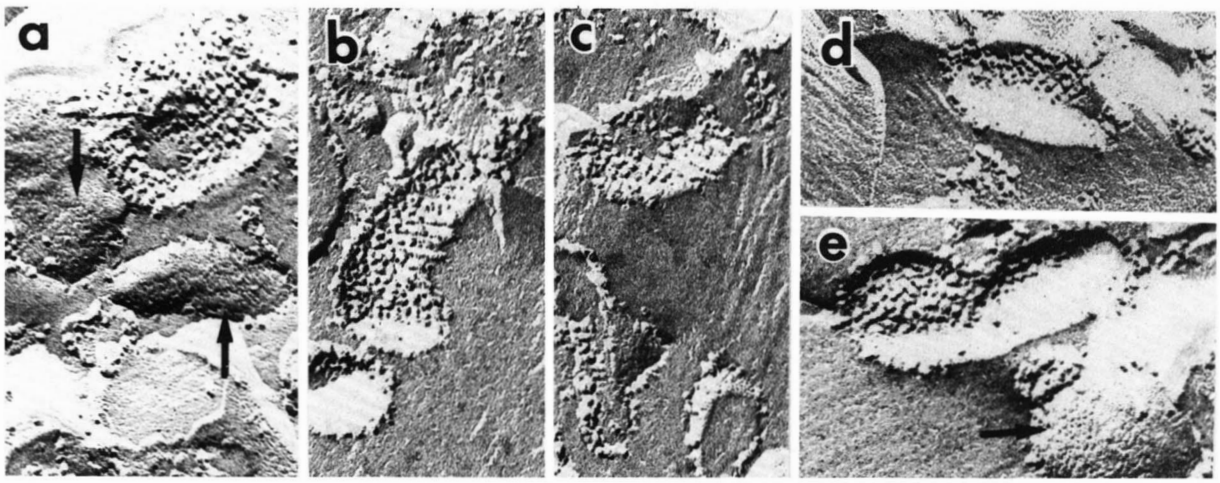


FIG. 5. **Freeze-fracture micrographs of sarcoplasmic reticulum membranes with $E_1$ crystals.** Sarcoplasmic reticulum vesicles were exposed to $10^{-5}$ M $PrCl_3$ for 24 h (*a–c*) and to 0.5 mM $CaCl_2$ for 8 h (*d* and *e*) in the presence of 0.1 M KCl, 10 mM imidazole, pH 8.0, and 5 mM $MgCl_2$ at 2 °C. In the case of $Ca^{2+}$, 0.5 mM EGTA was included in the incubation medium so that free $Ca^{2+}$ was about 1–3 μM. The P face of the vesicles shows particles oriented obliquely in a crystalline array. Particles are spaced at about 60–70 Å apart along both axes of the crystal lattice. Individual obliquely oriented pits on the E face are also visible (*a*, *e*, *arrows*). Direction of shadowing is from below. Magnification: times 125,500.

### *The Structure of the Crystals*

As observed by negative stain electron microscopy, the $E_1$ crystals are strikingly different from the previously described $E_2$ crystals induced by vanadate (Dux and Martonosi, 1983a, 1983b, 1983c, 1983d; Taylor *et al.*, 1984). The $E_2$ crystals contain dimers of the enzyme as structural units. The dimers are arranged in long chains which themselves are stable structural entities. The dimer chains wind helically around the long axis of the membrane tubules in a right-hand sense. The resulting lattice in projection has cell dimensions of $a$ = 65.9 Å, $b$ = 114.4 Å, and $\gamma$ = 77.9° (Taylor *et al.*, 1984). Similarly, freeze-fracture electron microscopy of the $E_2$ crystals show distinct parallel ridges 110 Å wide on the P face (protoplasmic) and complementary furrows on the E face (luminal) (Peracchia *et al.*, 1984).

Diffraction patterns calculated from densitometered images of the $E_1$ crystals show the first order spots from the near and far sides of the flattened tubule (Fig. 2). Often the second order of $a^*$ is visible at a resolution of about 30 Å. Higher order spots are not usually seen due to the relatively poor order in the crystals. The cell constants of the $E_1$ crystals formed with 3 different lanthanide ions are in agreement within experimental error (Table I) and are consistent at this resolution, with a single unit cell representing all three forms, and by implication a similar structure. The unit cell is oriented with the $a$ axis about 70–80° to the tubule axis, depending upon the width of the tubule. The unit cell dimensions are consistent with there being only one $Ca^{2+}$-ATPase molecule/unit cell.

Density maps at about 30-Å resolution of the structure in projection (Fig. 6) show a pear-shaped profile similar to that observed for the vanadate-induced crystals (Taylor *et al.*, 1984). From the three-dimensional reconstruction (Taylor *et al.*, 1985) we know that this pear-shaped profile arises from the shape of the cytoplasmic region of the molecule. The long axis of the molecule is oriented roughly perpendicular to the $b$ axis of the unit cell. This places it between 50 and 60° to the tubule axis. In this respect the molecular orientation is similar to that of the vanadate-induced crystals, the major difference being the lack of antiparallel chains in the $E_1$ form.

TABLE I

*Cell constants for lanthanide-induced $Ca^{2+}$-ATPase crystals*

| | *a* | *b* | γ |
|---|---|---|---|
| Gadolinium[a] | 61.7 ± 5.1 | 54.4 ± 5.9 | 111.0 ± 6.6 |
| Lanthanum[b] | 71.9 ± 6.6 | 51.1 ± 5.1 | 103.8 ± 7.4 |
| Praseodymium[c] | 66.8 ± 3.8 | 50.4 ± 2.2 | 114.6 ± 2.4 |

[a] Average of 6 crystals.
[b] Average of 2 crystals.
[c] Average of 16 crystals.

### *Optimization of Experimental Conditions for the Induction of the $E_1$ Crystals of $Ca^{2+}$-ATPase by $Ca^{2+}$ and Lanthanides*

*$Ca^{2+}$ Concentration*—The presence of endogenous $Ca^{2+}$ in sarcoplasmic reticulum vesicles and in the solutions used for crystallization, dictated special conditions. The dependence of $Ca^{2+}$-induced crystallization on $Ca^{2+}$ concentration was investigated in two types of systems. (*a*) Following Chelex treatment of the vesicles and solutions, to minimize endogenous $Ca^{2+}$ levels, $Ca^{2+}$ was added to the crystallization medium to final concentrations of 0.01–5 mM. (*b*) $Ca^{2+}$-EGTA buffer system was used to yield free $Ca^{2+}$ concentrations in the range of $10^{-9}$–$10^{-3}$ M.

In both systems the optimum $Ca^{2+}$ concentration required for crystallization was in the range of $10^{-5}$–$10^{-4}$ M. Since $10^{-5}$ M $Ca^{2+}$ is already effective in inducing $Ca^{2+}$-ATPase crystals at pH 8.0, in the presence of 0.1 M KCl, 10 mM imidazole, and 5 mM $MgCl_2$, it is not surprising that $E_1$-type crystals were occasionally observed in sarcoplasmic reticulum vesicles without addition of $Ca^{2+}$ or lanthanides.

*Lanthanide Concentration*—The effects of $GdCl_3$ and $PrCl_3$ were tested on Chelex-treated microsomes in the concentration range of $10^{-7}$–$10^{-4}$ M. Optimal crystallization was obtained with 6–8 μM lanthanide at a protein concentration of 1 mg/ml at pH 8.0 in a medium of 0.1 M KCl, 10 mM imidazole, 5 mM $MgCl_2$ at 2 °C. Below this concentration the frequency of crystalline vesicles declined presumably because there was less than 1 mol of lanthanide present per mol of $Ca^{2+}$-ATPase. At lanthanide concentrations in excess of $10^{-5}$ M aggregation of vesicles occurred, and the observation of crystalline arrays became technically more difficult. The optimal lanthanide

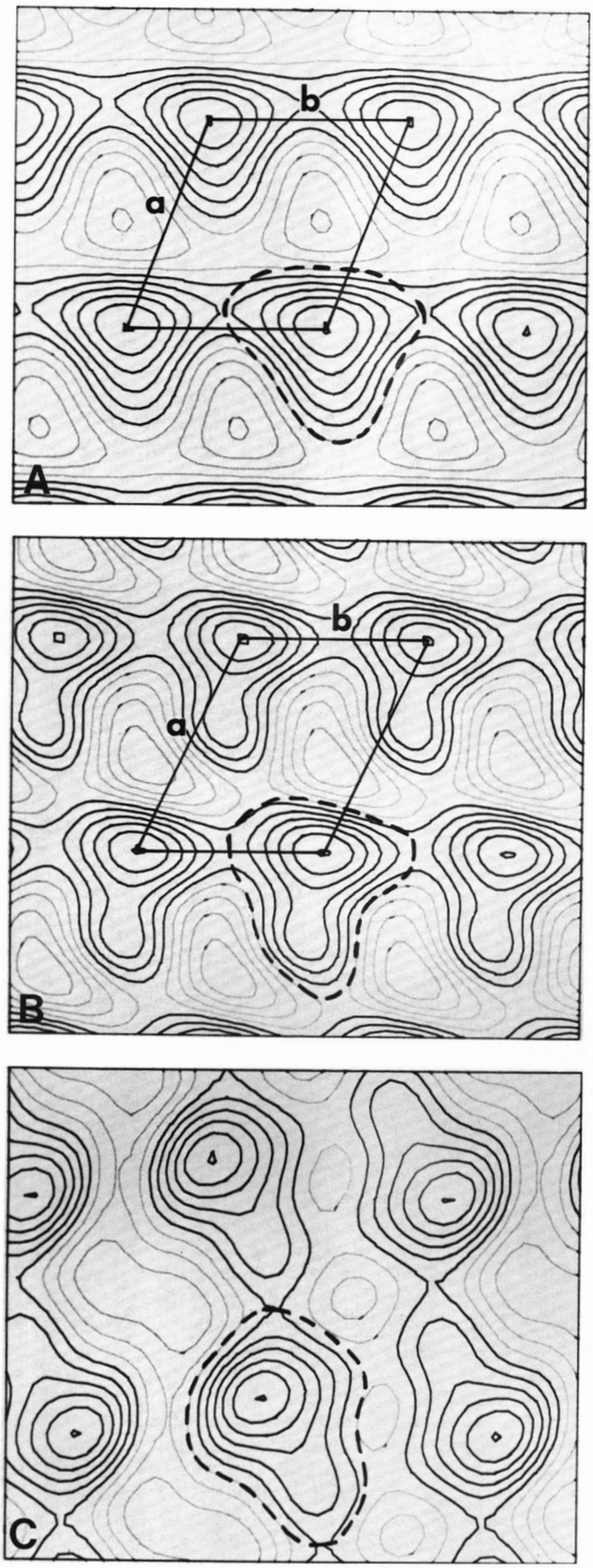


FIG. 6. **Isodensity contour maps of $E_1$ and $E_2$ crystals in projection at 30-Å resolution.** *a*, gadolinium-induced $E_1$ crystals. The unit cell is drawn and *a* and *b* axes are labeled. One molecule of $Ca^{2+}$-ATPase is outlined with the *dashed line*. Data used was an average of 6 crystals. *b*, praseodymium-induced $E_1$ crystals. Both $E_1$ crystal forms analyzed have approximately pear-shaped profiles in projection that are similar to that observed in vanadate-induced crystals. Data used is an average of 16 crystals. *c*, projection derived from vanadate-induced crystals (Taylor *et al.*, 1984) with one $Ca^{2+}$-ATPase molecule outlined with *dashed line*. In the vanadate crystals $Ca^{2+}$-ATPase molecules are arranged pair-wise in antiparallel chains. Map scale: 0.556 mm/Å.

concentration for crystallization (6–8 μM) is about 10 times lower than the optimal concentration of calcium. This is in agreement with the observations of Grisham (1982) that the affinity of $Gd^{3+}$ for the $Ca^{2+}$-ATPase is about 10 times greater than that of $Ca^{2+}$.

*Temperature and pH*—Optimum crystallization was obtained with $Ca^{2+}$ and lanthanides at 2 °C; few poorly organized crystals were formed at 25 °C and none at 37 °C. Slight alkalinity, pH 8.0, favored crystallization. Crystallization was poor at pH 7.0 and 9.0, and essentially no crystals were formed at pH 6.0 or 10.0. The effects of pH and temperature are consistent with the stabilization of the $E_1$ conformation of $Ca^{2+}$-ATPase at pH 8.0 and at low temperature (Pick and Karlish, 1982).

*Mg and KCl Concentration*—Optimum crystallization in the $E_1$ form required 0.1 M KCl and 5 mM $MgCl_2$. No crystals were obtained with 6 μM Pr at 0 or 0.6 M KCl in the presence of 5 mM $MgCl_2$, and only few crystals were formed with 0 or 20 mM $MgCl_2$ in the presence of 0.1 M KCl. Pretreatment of the vesicles and the crystallization media with Chelex chelating resin did not perceptibly affect the frequency or the quality of the crystals obtained with 10–100 μM Ca or with 6–8 μM Pr.

*The Effect of ATP and ATP Analogs*—ATP (5 mM) inhibited the $Ca^{2+}$-induced crystallization and disrupted $E_1$ crystals previously formed in the presence of 100 μM $CaCl_2$. In a few experiments crystalline arrays of ATPase molecules still developed in the presence of 6 μM $PrCl_3$ and 0.1–5 mM AMP-PCP or AMP-PNP. The effect of ATP analogs was not investigated in sufficient detail to permit statistical analysis of their influence on the extent of crystallization.

*Purified ATPase Preparations*—In purified ATPase vesicles, prepared according to MacLennan (1970), neither lanthanides nor calcium induced regularly the formation of $Ca^{2+}$-ATPase crystals. This is presumably due to the combined effects of residual detergents and the loss of polarity of ATPase molecules in reconstituted membranes.

$E_1$ crystals were readily induced by $PrCl_3$ in sarcoplasmic reticulum vesicles that were washed, without solubilization of the ATPase, with 0.1 mg of deoxycholate/mg of protein to remove extrinsic membrane proteins, followed by treatment with Bio-Bead SM-2 particles (20–50 mesh) to reduce the concentration of detergent. Without treatment with the hydrophobic resin the residual deoxycholate interfered with the crystallization.

*Fixation and Negative Staining Conditions*—In contrast to the $E_2$ crystals produced by vanadate in a $Ca^{2+}$-free medium, the $E_1$ crystals induced by $Pr^{3+}$ were only poorly preserved after fixation with 0.1–0.4% glutaraldehyde at 2 °C for 30 min.

Negative staining with uranyl acetate or uranyl formate at pH 4.3 produced better results than staining with K-phosphotungstate at pH 7.0, in spite of the favorable effect of alkaline pH on the formation of $E_1$ crystals. Less promising results were obtained with uranyl nitrate, that cannot penetrate across bilayer membranes (Ting-Beall, 1980).

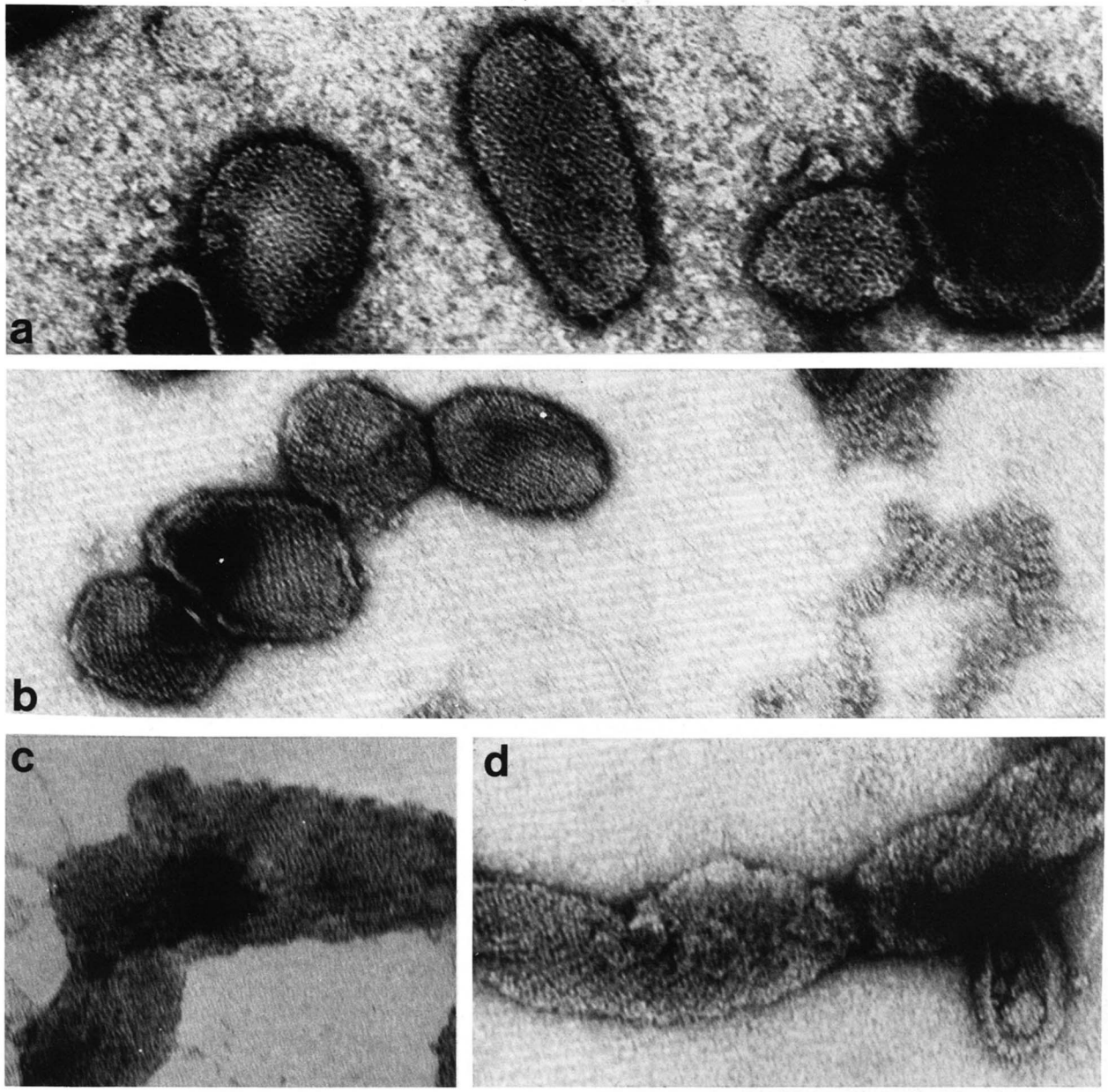


FIG. 7. **Repeated transformation of the $E_1$- into $E_2$-type crystals within the same sarcoplasmic reticulum preparation.** Sarcoplasmic reticulum vesicles were incubated at 2 °C for 16 h in a medium of 0.1 M KCl, 10 mM imidazole, pH 8.0, 5 mM $MgCl_2$, and 6 μM $PrCl_3$. The surface particles became ordered into $E_1$-type arrays (*a*). EGTA (0.5 mM) added to the same preparation destroyed the $E_1$ crystals within 1 h (not shown), and subsequent addition of $Na_3VO_4$ (5 mM) induced extensive formation of $E_2$-type crystals after 12 h (*b*). Next the $Pr^{3+}$ concentration was increased to 1 mM; after 4 h at 2 °C the $E_2$-type crystals were absent and among the aggregated vesicles poorly ordered $E_1$-type crystals appeared again (*c*). This observation implies that $Pr^{3+}$ is able to override the effect of $Na_3VO_4$ on the conformational equilibrium of the $Ca^{2+}$-ATPase. EGTA (5 mM) added to this sample immediately dispersed the aggregates into isolated vesicles and after 4 h at 2 °C, massive reformation of the $E_2$-type crystals was induced by the 5 mM $Na_3VO_4$ already present in the sample (*d*). According to sodium dodecyl sulfate-polyacrylamide gel electrophoresis, the protein composition of the sample remained unchanged throughout the procedure. All specimens were negatively stained with 1% uranyl acetate. Magnification: times 200,000.

### *Reversible Interconversion of the $Ca^{2+}$-ATPase between the $E_1$ and $E_2$ Crystal Forms*

By proper selection of the experimental conditions, a reversible interconversion between the two crystal forms ($E_1$ and $E_2$) can be observed.

$E_1$-type $Ca^{2+}$-ATPase crystals were formed by incubation of Chelex-treated sarcoplasmic reticulum vesicles with 6 μM $PrCl_3$ for 16 h at 2 °C (Fig. 7*a*). Addition of 0.5 mM EGTA to these vesicles caused the rapid disappearance of the $E_1$ crystals, and typical $E_2$ crystals formed 15 h after addition of 5 mM $Na_3VO_4$ (Fig. 7*b*). The vanadate-induced $E_2$ crystals were disrupted by $PrCl_3$ (1 mM) and a somewhat disorganized $E_1$ lattice reappeared (Fig. 7*c*). Aggregation of the vesicles in the presence of $PrCl_3$ made the observation of the crystals difficult. EGTA in a concentration sufficient to chelate $Pr^{3+}$ (5 mM) dissolved the macroscopic vesicle aggregates, destroyed the $E_1$ lattice, and together with the 5 mM vanadate already present, caused the reformation of the $E_2$ crystals (Fig. 7*d*). Glutaraldehyde fixation of the $E_1$ crystals induced by $Pr^{3+}$

FIG. 8. **$Ca^{2+}$-ATPase crystals in the presence of Cr(III)-ATP and $Ca^{2+}$.** The Cr(III)-ATP was prepared according to Dunaway-Mariano and Cleland (1980). Free Cr(III) was removed by treatment with Chelex 100 chelating resin, followed by elution of Cr(III)-ATP from a Dowex 50 column using a saturated solution of aniline in water as eluant.[2] The middle portion of the eluate was used in the experiments. The crystals were formed in sarcoplasmic reticulum vesicles (1 mg of protein/ml), exposed to 0.1 mM Cr(III)-ATP at 2 °C for 16 h in a medium of 0.1 M KCl, 10 mM imidazole, pH 8.0, 5 mM $MgCl_2$, and $\simeq 10^{-5}$ M $CaCl_2$. Negative staining with 1% uranyl acetate at pH 4.3. Magnification: times 200,000.

stabilized the $E_1$-type arrays, that persisted in fixed preparations even after addition of 0.5 mM EGTA and 5.0 mM $VO_4$.

The $Ca^{2+}$ concentration required for the formation of $E_1$-type crystals interferes with the vanadate-induced crystallization of the $Ca^{2+}$-ATPase in the $E_2$ form. The critical $Ca^{2+}$ concentration for this transition was established, using an EGTA buffer system, at about $10^{-6}$ M $Ca^{2+}$.

These experiments clearly demonstrate the reversible interconversion between the $E_1$ and $E_2$ crystal forms of the $Ca^{2+}$-ATPase and provide a striking illustration of the visible structural differences between the $E_1$ and $E_2$ crystals on the same microsome preparation.

### *The Effects of Chromium(III) and Chromium(III)-ATP Complex on the Crystallization of $Ca^{2+}$-ATPase in the Presence of $Ca^{2+}$*

The chromium(III) complex of ATP (DePamphilis and Cleland, 1973; Dunaway-Mariano and Cleland, 1980) has become a valuable dead-end inhibitor in the study of the kinetic mechanism of several enzymes (Young, 1975), including the $Ca^{2+}$ transport ATPase of sarcoplasmic reticulum (Serpersu *et al.*, 1982). The hydrolysis of Cr-ATP by the $Ca^{2+}$-ATPase leads to the formation of a stable phosphoenzyme, that binds $Ca^{2+}$ in an occluded form. The inhibition of $Ca^{2+}$ transport and ATP hydrolysis by Cr-ATP is due to the accumulation of this $E_1$(P, Cr-ATP)—2Ca intermediate (Serpersu *et al.*, 1982).

Since the stabilization of a particular conformation of the $Ca^{2+}$-ATPase plays a major role in the formation of $E_1$ crystals by $Ca^{2+}$ and lanthanides, and of the $E_2$ crystals by vanadate, we investigated the effects of Cr(III) and of the chromium(III)-ATP complex on the crystallization of $Ca^{2+}$-ATPase.

Sarcoplasmic reticulum vesicles were incubated in a medium of 0.1 M KCl, 10 mM imidazole, pH 8.0, 5 mM $MgCl_2$, and $\simeq 10^{-5}$ M $CaCl_2$ at 2 °C for 18 h. Crystalline arrays of ATPase molecules appeared on the surface of about 10–15% of the vesicles (Fig. 1). Addition of 0.1 mM Cr-ATP to the above system increased the frequency of crystalline arrays to such extent that within 24 h about 30–40% of the vesicles contained crystals (Fig. 8). The crystallization of $Ca^{2+}$-ATPase by Cr-ATP is dependent upon the presence of $Ca^{2+}$, since inclusion of 0.5 mM EGTA in the medium completely prevented the crystallization.

The visual appearance of the ATPase crystals induced by $Ca^{2+}$ (Fig. 1) and by $Ca^{2+}$ + Cr-ATP (Fig. 8) is similar and consistent with the suggestion that both crystals reflect the $E_1$ conformation of the $Ca^{2+}$-ATPase.

[2] W. W. Cleland, personal communication.

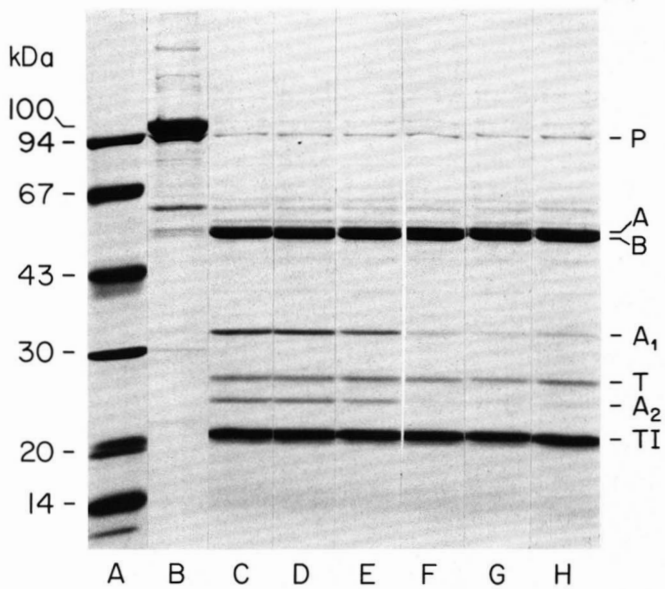


FIG. 9. **The effect of EGTA on the conformational equilibrium of $Ca^{2+}$-ATPase determined by tryptic hydrolysis.** Sarcoplasmic reticulum vesicles (2 mg of protein/ml) were treated overnight with Chelex resin particles (100 mg of wet resin/mg of protein) in a medium of 0.1 M KCl, 10 mM imidazole, pH 8.0. $MgCl_2$ (5 mM), $Na_3VO_4$ (1 mM), and EGTA were added and digestion was initiated by trypsin (0.1 mg/ml) at 25 °C. The cleavage was stopped 5 min later by soybean trypsin inhibitor in 2-fold excess over trypsin (0.2 mg/ml). The samples were solubilized and the proteins separated by sodium dodecyl sulfate-polyacrylamide gradient gel electrophoresis (6–18% gradient) as described earlier (Dux and Martonosi, 1983b). *A*, molecular weight markers (phosphorylase (94 kDa), bovine serum albumin (67 kDa), ovalbumin (43 kDa), carbonic anhydrase (30 kDa), trypsin inhibitor (20 kDa), α-lactalbumin (14 kDa)). *B*, control sarcoplasmic reticulum, without trypsin or trypsin inhibitor. The dense band at 100 kDa is the $Ca^{2+}$ transport ATPase. *P*, phosphorylase. *C—H*, complete systems with the following EGTA concentrations: ○ (*C*); $10^{-6}$ M (*D*); $5 \times 10^{-6}$ M (*E*); $10^{-5}$ M (*F*); $10^{-4}$ M (*G*); $10^{-3}$ M (*H*). Note that at least $10^{-5}$ M EGTA (*lane F*) is required for inhibition of the $T_2$ cleavage of the $Ca^{2+}$-ATPase, as shown by the virtual absence of the $A_1$ and $A_2$ fragments in *lanes F–H*. *T*, trypsin; *TI*, trypsin inhibitor. *A*, *B*, $A_1$, and $A_2$ denote the corresponding tryptic fragments of the $Ca^{2+}$-ATPase.

The optimal concentration of Cr-ATP for crystallization in the basic test medium of 0.1 M KCl, 10 mM imidazole, pH 8.0, 5 mM $MgCl_2$, and $10^{-5}$ M $CaCl_2$ was 0.1 mM. Fewer crystals were detected at 0.01 mM and very few at 1 or 5 mM Cr-ATP concentration. Maximum crystallization was usually reached within 1 day. The effect of other parameters was tested by varying the concentration of individual components of the basic system at 0.1 mM Cr-ATP concentration. The optimal $Mg^{2+}$ concentration was 5 mM, with fewer crystals at 0 or 20 mM $MgCl_2$. Although 0.1 M KCl produced the best results, crystallization definitely occurred at 0 and 0.6 M KCl concentration. The pH optimum was at pH 8.0, with sharp decline in crystallization at pH 7 and 9, and essentially no crystallization at pH 6.0. Although $Ca^{2+}$ was required for crystallization at a level of $\simeq 10^{-5}$ M, further increase in $[Ca^{2+}]$ to $10^{-4}$ M reduced the number of crystalline vesicles, and no crystals were detected in the presence of 1 mM $Ca^{2+}$ and 0.1 mM Cr-ATP. The optimum temperature for crystallization was 2 °C; fewer crystals were observed at 25 °C and no crystals at 37 °C. The sharp decline with temperature may not be a feature of the crystallization *per se* but could be due to denaturation or proteolysis of the $Ca^{2+}$-ATPase at elevated temperatures.

Surprisingly, in several control experiments 0.1 mM $CrCl_3$ also induced significant crystallization. For this reason it is not clear whether the effects of $Cr^{3+}$ and Cr(III)-ATP are attributable to the formation of a dead-end intermediate of $Ca^{2+}$-ATPase as described by Serpersu *et al.* (1982), or to the stabilization of the $Ca^{2+}$-induced crystals of $Ca^{2+}$-ATPase by some other mechanism.

### *The Effect of $Ca^{2+}$ and Lanthanides on the Tryptic Digestion Profiles of the $Ca^{2+}$-ATPase*

Trypsin preferentially cleaves the $Ca^{2+}$-ATPase of sarcoplasmic reticulum at the $T_1$ cleavage site into two major fragments, designated as fragment A and fragment B (MacLennan and Reithmeier, 1982). Further cleavage of fragment A at the $T_2$ cleavage site yields fragments $A_1$ and $A_2$. Previously we demonstrated (Dux and Martonosi, 1983b) that exposure of sarcoplasmic reticulum vesicles to vanadate in a calcium-free medium inhibits the cleavage of $Ca^{2+}$-ATPase by trypsin at the $T_2$ cleavage site, without interference with the initial cleavage at the $T_1$ site. The inhibition of tryptic cleavage by vanadate at the $T_2$ site is assumed to reflect the stabilization of the $E_2$ conformation of the $Ca^{2+}$-ATPase.

This effect of vanadate is extremely sensitive to trace $Ca^{2+}$ contamination. Even with Chelex-treated microsomes and buffer solution about $10^{-5}$ M EGTA is required, in addition to 5 mM $Na_3VO_4$, to prevent the cleavage of fragment A into the $A_1$ and $A_2$ subfragments (Fig. 9). Addition of $Ca^{2+}$ (Fig. 10) or $Pr^{3+}$ (Fig. 11) relieves the inhibition caused by vanadate and EGTA as shown by the appearance of the $A_1$ and $A_2$ fragments at cation concentrations in slight excess over EGTA. We assume that $Ca^{2+}$ and $Pr^{3+}$ shift the equilibrium from the $E_2$ in favor of the $E_1$ conformation, and thereby facilitate the attack of trypsin at the $T_2$ site. Other lanthanides, with slight

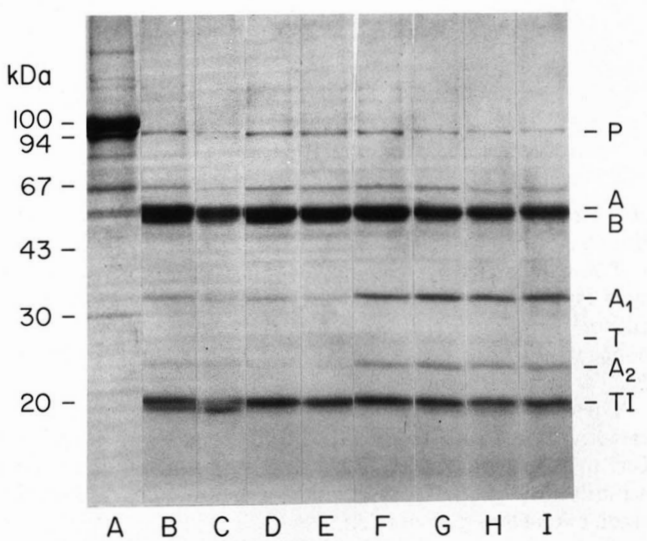


FIG. 10. **The effect of $[Ca^{2+}]$ on the tryptic cleavage of $Ca^{2+}$-ATPase in the presence of $Na_3VO_4$.** Sarcoplasmic reticulum vesicles (2 mg of protein/ml) were pretreated with Chelex as described in the legend to Fig. 9; 5 mM $MgCl_2$, 0.1 mM $Na_3VO_4$, and $5 \times 10^{-5}$ M EGTA were added together with $CaCl_2$ in final concentrations (M) of ○ (*B*); $10^{-6}$ (*C*); $5 \times 10^{-6}$ (*D*); $10^{-5}$ (*E*); $5 \times 10^{-5}$ (*F*); $10^{-4}$ (*G*); $5 \times 10^{-4}$ (*H*); and $10^{-3}$ (*I*), and incubated for 30 min at 25 °C. The tryptic digestion and the gel electrophoresis of the samples were carried out as described in the legend to Fig. 9. $Ca^{2+}$ in a concentration equal to or exceeding that of the EGTA (50 μM, *lanes F–I*) can overcome the inhibitory effect of $VO_4$ on trypsin cleavage at the second ($T_2$) cleavage site, and the tryptic digestion of the $Ca^{2+}$-ATPase proceeds with the formation of $A_1$ and $A_2$ subfragments in *lanes F–I*. For other details see text and the legend of Fig. 9. *Lane A*, control sample without trypsin and trypsin inhibitor. *P*, phosphorylase; *T*, trypsin; *TI*, trypsin inhibitor.

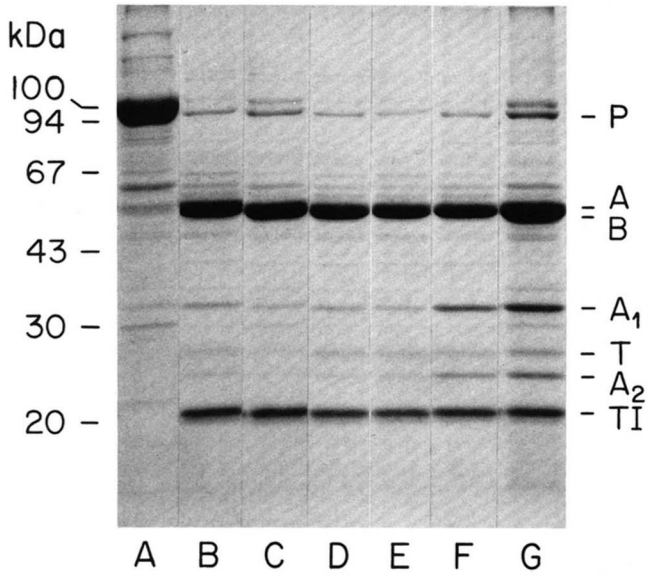


FIG. 11. **The effect of $Pr^{3+}$ on the tryptic cleavage of the $Ca^{2+}$-ATPase in the presence of $Na_3VO_4$.** The experimental procedure was as described in the legend to Fig. 10, except $Ca^{2+}$ was replaced by $PrCl_3$ in concentrations of $10^{-6}$ M (*C*), $10^{-5}$ M (*D*), $5 \times 10^{-5}$ M (*E*), $10^{-4}$ M (*F*), and $10^{-3}$ M (*G*) in the incubating media. *Lane A*, control sample without trypsin inhibitor, EGTA or Pr. *Lane B*, control sample without $Pr^{3+}$ but with trypsin (T), trypsin inhibitor (*TI*), and EGTA. In the presence of $5 \times 10^{-5}$ M EGTA, $10^{-4}$ M $Pr^{3+}$ was able to convert the enzyme from the $VO_4$-induced $E_2$ into the $E_1$ conformation, as reflected by the appearance of $A_1$ and $A_2$ subfragments in *lanes F* and *G*. The relatively high concentration of Pr ($10^{-4}$ M) required to alter the digestion pattern, as compared with the 6–8 $\mu$M needed for crystallization (see Fig. 4), is attributable in part to the presence of 50 $\mu$M EGTA, that chelates much of the added $Pr^{3+}$. For other details see text and the legends of Figs. 9 and 10.

variations in effectiveness, gave similar results (Fig. 12). These effects may be due, either to binding of lanthanides to the high affinity $Ca^{2+}$ binding site of the $Ca^{2+}$-ATPase, or to a site distinct from that of $Ca^{2+}$ (Itoh and Kawakita, 1984). $Ca^{2+}$ released from EGTA by lanthanides may contribute to the observations. Further experiments are needed to resolve these ambiguities.

Prior cleavage of the $Ca^{2+}$-ATPase by trypsin into the two major fragments (A and B) did not interfere with the formation of $E_1$ crystals by $Pr^{3+}$ (Fig. 13), but further cleavage of the ATPase at the $T_2$ site inhibited crystallization.

### *The Effect of Membrane Potential on the Formation of $E_1$ Crystals*

Inside positive membrane potential generated by dilution of sarcoplasmic reticulum vesicles from choline chloride into a K-glutamate medium promoted the formation of $E_2$ crystals of $Ca^{2+}$-ATPase in the presence of EGTA and vanadate (Dux and Martonosi, 1983d; Beeler *et al.*, 1984). Substitution of K-glutamate for choline chloride produced negative potential, and disrupted the preformed $E_2$ crystals of the $Ca^{2+}$-ATPase (Dux and Martonosi, 1983d). These observations suggested that inside-positive potential stabilizes the $E_2$, while negative potential stabilizes the $E_1$ conformation of the $Ca^{2+}$-ATPase.

If these assumptions are correct, it is expected that negative potential would promote the formation of the $E_1$ crystals of $Ca^{2+}$-ATPase in the presence of 6 $\mu$M $Pr^{3+}$. The experiment described in Fig. 14 shows that this is indeed the case. Significant crystallization of the $Ca^{2+}$-ATPase was obtained within 30 s after dilution of the vesicles equilibrated with K-glutamate into a choline chloride medium containing 6 $\mu$M $PrCl_3$ (Fig. 14). Similar degree of crystallization in vesicles diluted from choline chloride into choline chloride or from K-glutamate into K-glutamate medium required several hours of incubation. Since ion substitution of this type generates inside negative potential (Beeler *et al.*, 1981, 1984; Martonosi, 1984),

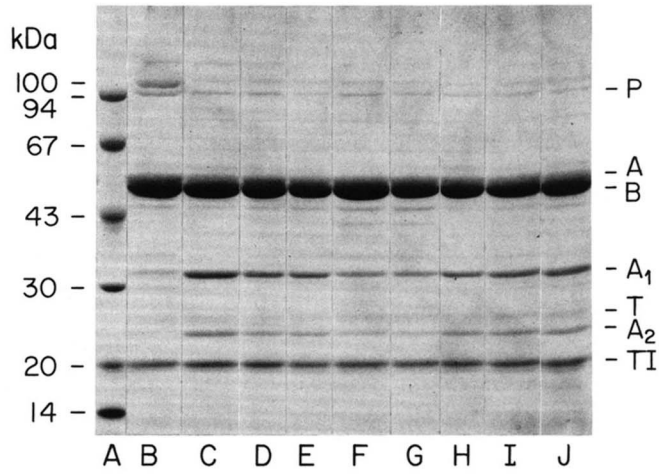


FIG. 12. **The effect of different lanthanides and $Ca^{2+}$ on the $VO_4$-induced tryptic cleavage pattern of sarcoplasmic reticulum $Ca^{2+}$-ATPase.** Microsome samples were treated with Chelex as described in the legend to Fig. 9; 5 mM $MgCl_2$, 0.1 mM $VO_4$, and $5 \times 10^{-5}$ M EGTA were added in the presence of $7.5 \times 10^{-5}$ M Ca (*C*), $La^{3+}$ (*D*), $Pr^{3+}$ (*E*), $Nd^{3+}$ (*F*), $Gd^{3+}$ (*G*), $Tb^{3+}$ (*H*), $Ho^{3+}$ (*I*), and $Yb^{3+}$ (*J*) after incubation for 30 min at 25 °C. Tryptic cleavage and gel electrophoresis of the samples was carried out as described in the legend to Fig. 9. *Lane A*, molecular weight markers: *lane B*, control sample without $Ca^{2+}$ or lanthanides, but with trypsin, $Na_3VO_4$, and trypsin inhibitor. For other details see legends to Figs. 9 and 10.

FIG. 13. **Crystallization of the $Ca^{2+}$-ATPase by $PrCl_3$ after tryptic cleavage into the A and B fragments.** Sarcoplasmic reticulum vesicles were treated with Chelex and subjected to tryptic hydrolysis for 5 min at 25 °C in a medium of 0.1 M KCl, 10 mM imidazole, pH 8.0, and 5 mM $MgCl_2$, essentially as described in the legend to Fig. 9. The hydrolysis was stopped with trypsin inhibitor (0.2 mg/0.1 mg of trypsin), and $PrCl_3$ (6 $\mu$M) was added to initiate crystallization at 2 °C. After 16 h, samples were analyzed by sodium dodecyl sulfate-polyacrylamide gel electrophoresis. It was ascertained that complete cleavage of the $Ca^{2+}$-ATPase into A and B subunits has taken place, with only slight additional cleavage at the $T_2$ site into $A_1$ and $A_2$ subunits. Samples were negatively stained with 1% uranyl acetate for electron microscopy. Magnification: times 175,000.

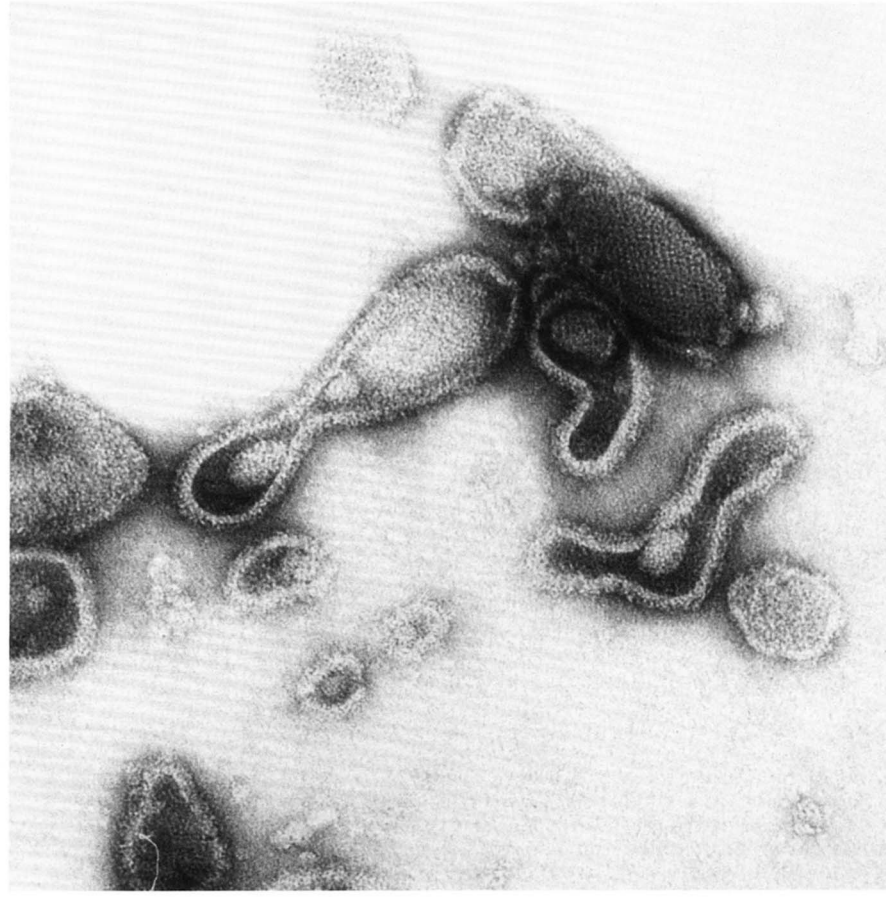

FIG. 14. **The effect of membrane potential on the rate of crystallization of $Ca^{2+}$-ATPase induced by $PrCl_3$.** Sarcoplasmic reticulum vesicles (25 mg of protein/ml) were equilibrated with a medium of 0.15 M K-glutamate, 10 mM imidazole, pH 8.0, and 5 mM $MgCl_2$ for 18 h at 2 °C. Inside negative potential was generated and crystallization was initiated by dilution of the vesicles into a medium of 0.15 M choline chloride, 10 mM imidazole, pH 8.0, 5 mM $MgCl_2$, and 6 $\mu$M $PrCl_3$, at 2°C. Sample was taken for negative staining with 1% uranyl acetate 30 s after dilution. Magnification: times 200,000.

we propose that negative potential promotes the formation of $E_1$ crystals, presumably by stabilizing the $E_1$ conformation of the $Ca^{2+}$-ATPase.

## DISCUSSION

Two-dimensional crystalline arrays of $Ca^{2+}$-ATPase molecules develop in sarcoplasmic reticulum vesicles exposed to 10–100 $\mu$M $Ca^{2+}$ or to one of several lanthanide ions (La, Gd, Pr, Nd, Tb, Yb, Ho) at 6–8 $\mu$M concentration.

The concentration of $Ca^{2+}$ required for optimum crystallization is sufficient to saturate the high affinity $Ca^{2+}$ binding sites of the $Ca^{2+}$-ATPase (Martonosi and Beeler, 1983). The susceptibility of the $Ca^{2+}$-ATPase to proteolytic cleavage, together with kinetic and spectroscopic evidence (Pick and Karlish, 1982; Andersen *et al.*, 1982) provide reasonable basis to assume that under the conditions of crystallization by $Ca^{2+}$ the enzyme is stabilized in the $E_1$ conformation.

Lanthanide ions are usually perceived as $Ca^{2+}$ analogs (Martin and Richardson, 1979), and earlier literature on the effects of lanthanides on the $Ca^{2+}$-ATPase is consistent with competition by lanthanides for the high affinity $Ca^{2+}$ binding site on the $Ca^{2+}$-ATPase (Chevallier and Butow, 1971; Yamada and Tonomura, 1972; Krasnow, 1972, 1977; dos Remedios, 1977; Chiesi and Inesi, 1979; Stephens and Grisham, 1979; Highsmith and Head, 1983). Therefore it is reasonable to assume that lanthanides also favor the accumulation of the $E_1$ enzyme form. According to Stephens and Grisham (1979; see, however, Itoh and Kawakita, 1984), the affinity of $Gd^{3+}$ for the $Ca^{2+}$-ATPase is 10 times greater than that of $Ca^{2+}$. This would explain the observation that optimum crystallization by lanthanides was obtained near 1:1 molar stoichiometry with the $Ca^{2+}$-ATPase. The relatively sharp optimum at 6–8 $\mu$M lanthanide concentration is due to incomplete saturation of the binding site below and an abrupt change in the surface charge density of the membrane above the 1:1 lanthanide:ATPase molar ratio. Macroscopic aggregation of vesicles was observed at or above 10 $\mu$M lanthanide concentration.

The interaction of lanthanides with enzymes is a complex function of ionic radius, coordination geometry, and charge (Martin and Richardson, 1979). For this reason it is not surprising that a large number of lanthanides, $La^{3+}$, $Pr^{3+}$, $Nd^{3+}$, $Gd^{3+}$, $Tb^{3+}$, $Ho^{3+}$, and $Yb^{3+}$, listed in decreasing order of their ionic radii, were found to be effective in inducing crystallization of the $Ca^{2+}$-ATPase, and that $Pr^{3+}$, with an ionic radius closest to that of $Ca^{2+}$, was only slightly favored.

The $E_1$ and $E_2$ crystal forms have some similarities and some striking differences. Both crystal forms tend to assume elongated tubular shapes of similar diameters. In addition, the orientation of the $Ca^{2+}$-ATPase monomer relative to the tubule axis is nearly the same in both cases. Both the $E_1$ and $E_2$ crystal forms show an approximately pear-shaped profile for the $Ca^{2+}$-ATPase in projection. In view of the relatively low resolution available at the present time and the lack of a three-dimensional structure for the $E_1$ crystals, it would be premature to comment in detail on the significance of the differences in the projected structure seen in the density maps thus far calculated. The significant difference between the two crystal forms lies in their oligomeric association. $E_2$ crystals consist of dimers of the enzyme arranged in long chains (Taylor *et al.*, 1984). No dimers are observed in the $E_1$ crystals. The differences both in oligomeric association and in unit cell dimension suggest significant changes in the structure of the $Ca^{2+}$-ATPase on conversion between the $E_1$

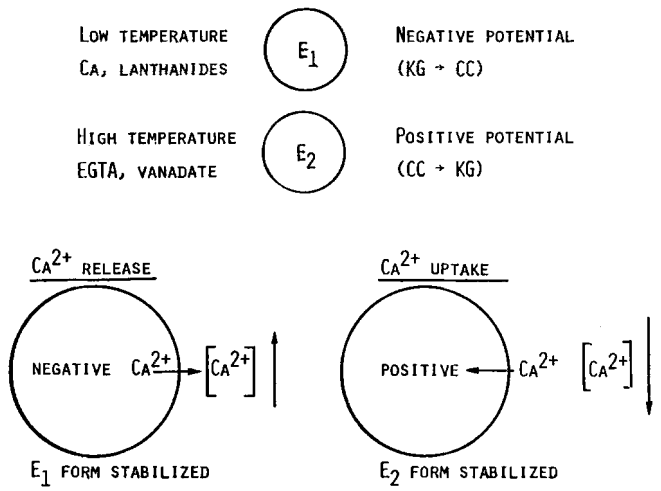


FIG. 15. **A summary of conditions that affect the conformational equilibrium ($E_1/E_2$) of $Ca^{2+}$-ATPase.** Negative potential is generated by $Ca^{2+}$ release or substitution of K-glutamate (*KG*) to choline chloride (*CC*) medium. Positive potential is generated during active $Ca^{2+}$ transport and by substitution of choline chloride to K-glutamate medium. For other details, see text.

and $E_2$ enzyme conformations during $Ca^{2+}$ transport.

Detailed structural studies of the $E_1$ crystals are in progress. Since the $E_1$ and $E_2$ conformations represent the structures of the $Ca^{2+}$ pump at the beginning and at the end of the $Ca^{2+}$ transport cycle, high resolution analysis of these crystals by reconstruction techniques may provide the much needed structural information about the molecular basis of $Ca^{2+}$ translocation. Such information usefully complements the static and time-resolved structural studies of the same system by x-ray and neutron diffraction techniques (Blasie *et al.*, 1982).

The lanthanide- or $Ca^{2+}$-induced formation of $E_1$ crystals, similarly to actin polymerization, may represent a form of fibrous condensation (Oosawa and Asakura, 1975), in which the concentration of protein polymers is determined by a "critical protein concentration." If the critical protein concentration for the formation of the $Ca^{2+}$- or lanthanide-induced crystals is close to the concentration of $Ca^{2+}$-ATPase in the sarcoplasmic reticulum this may explain the fact that, even under optimal conditions, crystals appear only in about 20–30% of the vesicle population. By contrast, the $E_2$ crystals produced by vanadate develop in 70–90% of the vesicles (Varga *et al.*, 1985), perhaps because the critical protein concentration for this process is below the concentration of the $Ca^{2+}$-ATPase in the sarcoplasmic reticulum. The relevant ATPase concentration in this respect is the concentration of the enzyme form ($E_1$ or $E_2$) that is actually involved in the crystallization process. Loomis *et al.* (1982) proposed that the equilibrium constant $E_2/E_1$ is of the order of $10^3$ or higher at pH 6.2 and 25 °C. This explains why the $Ca^{2+}$ or lanthanide crystals have not been observed under these conditions. The $E_2/E_1$ equilibrium shifts in favor of the $E_1$ conformation at pH 8.0 and low temperature (Pick and Karlish, 1982), providing optimum conditions for crystallization of the $Ca^{2+}$-ATPase in the $E_1$ form.

The transport and release of $Ca^{2+}$ by sarcoplasmic reticulum generate transient inside positive and inside negative membrane potentials, respectively (Martonosi, 1984). The positive potential promotes the formation of $E_2$ crystals of the $Ca^{2+}$-ATPase (Dux and Martonosi, 1983d; Beeler *et al.*, 1984), while negative potential favors the development of $E_1$ crystals. Positive potential inhibits and negative potential activates the $Ca^{2+}$ transport (Beeler *et al.*, 1981). These and other observations (Copeland *et al.*, 1984; Blumenthal *et al.*, 1984) indicate that membrane potential significantly affects the folding and interactions of membrane proteins, with changes in their enzymatic activity.

The effect of membrane potential on the conformation of $Ca^{2+}$-ATPase and on the interaction between ATPase molecules may have physiological significance. The release of $Ca^{2+}$ during muscle contraction generates negative potential across the sarcoplasmic reticulum (Martonosi, 1984) and increases the cytoplasmic [$Ca^{2+}$], creating conditions in activated muscle that favor the $E_1$ conformation (Fig. 15). Active transport of $Ca^{2+}$ into sarcoplasmic reticulum during relaxation may shift the equilibrium in favor of the $E_2$ form (Fig. 15), by generating positive potential and by lowering the cytoplasmic [$Ca^{2+}$] to $\simeq 10^{-8}$ M, where phosphate- or vanadate-induced $E_2$-type crystals of $Ca^{2+}$-ATPase have been observed (Dux and Martonosi, 1983c). The changes in membrane potential and cytoplasmic [$Ca^{2+}$] may affect significantly the $E_2$:$E_1$ ratio, and the monomer-oligomer equilibrium of the $Ca^{2+}$-ATPase, even if the development of crystalline ATPase arrays *in vivo* is prevented by cyclic changes in enzyme conformation connected with ATP hydrolysis.

*Acknowledgment*—Our thanks are due to Dr. Sandor Papp for the Cr(III)-ATP preparation used in some of the experiments.

## REFERENCES

Andersen, J. P., Møller, J. V., and Jørgensen, P. L. (1982) *J. Biol. Chem.* **257,** 8300–8307
Beeler, T. J., Farmen, R. H., and Martonosi, A. (1981) *J. Membr. Biol.* **62,** 113–137
Beeler, T. J., Dux, L., and Martonosi, A. (1984) *J. Membr. Biol.* **78,** 73–79
Blasie, J. K., Herbette, L., Pierce, D., Pascolini, A., Scarpa, A., and Fleischer, S. (1982) *Ann. N. Y. Acad. Sci.* **402,** 478–484
Blumenthal, R., Kempf, C., Vanrenswoude, J., Weinstein, J. N., and Klausner, R. D. (1984) *CETUS-UCLA Symp. Mol. Cell. Biol. New Ser.* **15,** 1–14
Chevallier, J., and Butow, R. A. (1971) *Biochemistry* **10,** 2733–2737
Chiesi, M., and Inesi, G. (1979) *J. Biol. Chem.* **254,** 10370–10377
Copeland, B. R., Landick, R., Nazos, P. M., and Oxender, D. L. (1984) *J. Cell. Biochem.* **24,** 345–356
Costello, M. J., and Corless, J. M. (1978) *J. Microsc. (Oxf.)* **112,** 17–37
DePamphilis, M. L., and Cleland, W. W. (1973) *Biochemistry* **12,** 3714–3724
dos Remedios, C. (1977) *J. Biochem. (Tokyo)* **81,** 703–708
Dunaway-Mariano, D., and Cleland, W. W. (1980) *Biochemistry* **19,** 1496–1505
Dupont, Y., Bennett, N., and Lacapere, J.-J. (1982) *Ann. N. Y. Acad. Sci.* **402,** 569–572
Dux, L., and Martonosi, A. (1983a) *J. Biol. Chem.* **258,** 2599–2603
Dux, L., and Martonosi, A. (1983b) *J. Biol. Chem.* **258,** 10111–10115
Dux, L., and Martonosi, A. (1983c) *J. Biol. Chem.* **258,** 11896–11902
Dux, L., and Martonosi, A. (1983d) *J. Biol. Chem.* **258,** 11903–11907
Dux, L., and Martonosi, A. (1984) *Eur. J. Biochem.* **141,** 43–49
Dux, L., Taylor, K. A., and Martonosi, A. (1984) *Fed. Proc.* **43,** 1700
Grisham, C. M. (1982) in *Membranes and Transport* (Martonosi, A., ed) Vol. 1, pp. 585–592, Plenum Publishing Corp., New York
Highsmith, S. R., and Head, M. R. (1983) *J. Biol. Chem.* **258,** 6858–6862
Ikemoto, N. (1982) *Annu. Rev. Physiol.* **44,** 297–317
Inesi, G., Watanabe, T., Coan, C., and Murphy, A. (1982) *Ann. N. Y. Acad. Sci.* **402,** 515–534
Itoh, N., and Kawakita, M. (1984) *J. Biochem. (Tokyo)* **95,** 661–669
Krasnow, N. (1972) *Biochim. Biophys. Acta* **282,** 187–194
Krasnow, N. (1977) *Arch. Biochem. Biophys.* **181,** 322–330
Loomis, C. R., Martin, D. W., McCaslin, D. R., Tanford, C. (1982) *Biochemistry* **21,** 151–156
Lowry, O. H., Rosebrough, N. J., Farr, A. L., and Randall, R. J. (1951) *J. Biol. Chem.* **193,** 265–275
MacLennan, D. H. (1970) *J. Biol. Chem.* **245,** 4508–4518

MacLennan, D. H., and Reithmeier, R. A. F. (1982) in *Membranes and Transport* (Martonosi, A., ed) Vol. 1, pp. 567–571, Plenum Publishing Corp., New York
Martin, R. B., and Richardson, F. S. (1979) *Q. Rev. Biophys.* **12,** 181–209
Martonosi, A. (1982) in *Calcium and Cell Function* (Cheung, W. Y., ed) Vol. 3, pp. 37–102, Academic Press, New York
Martonosi, A. (1984) *Physiol. Rev.* **65,** 1240–1320
Martonosi, A. N., and Beeler, T. J. (1983) in *Handbook of Physiology, Skeletal Muscle* (Peachey, L. D., Adrian, R. H., and Geiger, S. R., eds) pp. 417–485, American Physiological Society, Bethesda
Martonosi, A., Kracke, G., Taylor, K. A., Dux, L., and Peracchia, C. (1985) in *Regulation and Development of Membrane Transport Processes* (Graves, J. S., ed) pp. 57–85, John Wiley and Sons, New York
Nakamura, H., Jilka, R. L., Boland, R., and Martonosi, A. (1976) *J. Biol. Chem.* **251,** 5414–5423
Oosawa, F., and Asakura, S. (1975) *Thermodynamics of the Polymerization of Protein*, Academic Press, New York
Peracchia, C., Dux, L., and Martonosi, A. (1984) *J. Muscle Res. Cell Motil.* **5,** 431–442
Pick, U. (1982) *J. Biol. Chem.* **257,** 6111–6119
Pick, U., and Karlish, S. J. D. (1982) *J. Biol. Chem.* **257,** 6120–6126
Serpersu, E. H., Kirch, U., and Schoner, W. (1982) *Eur. J. Biochem.* **122,** 347–354
Stephens, E. M., and Grisham, C. M. (1979) *Biochemistry* **18,** 4876–4885
Stephens, E. M., and Grisham, C. M. (1980) *Fed. Proc.* **39,** 603
Taylor, K. A., Dux, L., and Martonosi, A. (1984) *J. Mol. Biol.* **174,** 193–204
Taylor, K. A., Dux, L., and Martonosi, A. (1985) *J. Mol. Biol.*, in press
Ting-Beall, H. P. (1980) *J. Micros.* **118,** 221–227
Yamada, S., and Tonomura, Y. (1972) *J. Biochem. (Tokyo)* **72,** 417–425
Young, R. G. (1975) *Adv. Enzymol.* **43,** 1–56
Varga, S., Csermely, P., and Martonosi, A. (1985) *Eur. J. Biochem.* **148,** 119–126